Original Article

The influence of MgO on the radiation protection and mechanical properties of tellurite glasses

M.Y. Hanfi [a, b, *], M.I. Sayyed [c, d], E. Lacomme [e], I. Akkurt [f], K.A. Mahmoud [a, b]

[a] Ural Federal University, St. Mira, 19, 620002, Yekaterinburg, Russia
[b] Nuclear Materials Authority, Maadi, Cairo, Egypt
[c] Department of Physics, Faculty of Science, Isra University, Amman, Jordan
[d] Department of Nuclear Medicine Research, Institute for Research and Medical Consultations (IRMC), Imam Abdulrahman Bin Faisal University (IAU), P.O. Box 1982, Dammam, 31441, Saudi Arabia
[e] Advanced Science Research, Junior, Eastchester High School, Eastchester, NY, United States
[f] Physics Department, Suleyman Demirel University, Isparta, Turkey

ARTICLE INFO

ABSTRACT

Mechanical moduli, such as Young's modulus (E), Bulks modulus (B), Shear modulus (S), longitudinal modulus (L), Poisson's ratio (σ) and micro Hardness (H) were theoretically calculated for $(100-x)TeO_2+x$ MgO glasses, where x = 10, 20, 30, 40 and 45 mol%, based on the Makishima–Mackenzie model. The estimated results showed that the mechanical moduli and the microhardness of the glasses were improved with the increase of the MgO contents in the TM glasses, while Poisson's ratio decreased with the increase in MgO content. Moreover, the radiation shielding capacity was evaluated for the studied TM glasses. Thus, the linear attenuation coefficient (LAC), mass attenuation coefficient (MAC), transmission factor (TF) and half-value thickness ($\Delta_{0.5}$) were simulated for gamma photon energies between 0.344 and 1.406 MeV. The simulated results showed that glass TM10 with 10 mol % MgO possess the highest LAC and varied in the range between 0.259 and 0.711 cm^{-1}, while TM45 glass with 45 mol % MgO possess the lowest LAC and vary in the range between 0.223 and 0.587 cm^{-1} at gamma photon energies between 0.344 and 1.406 MeV. Furthermore, the BXCOM program was applied to calculate the effective atomic number (Z_{eff}), equivalent atomic number (Z_{eq}) and buildup factors (EBF and EABF) of the glasses. The effective removal cross-section for the fast neutrons (ERCSFN, $\sum_R$) was also calculated theoretically. The received data depicts that the lowest $\sum_R$ was achieved for TM10 glasses, where $\sum_R = 0.0193$ cm^2 g^{-1}, while TM45 possesses the highest ERCSFN where $\sum_R = 0.0215$ cm^2 g^{-1}.

1. Introduction

As technologies that implement radiation become more common, more materials that protect people from exposure to radiation are developed. These radiation shields absorb high energy photons that could otherwise severely cause permanent damage to cells in the human body. Long-term exposure to high energy radiation can lead to tissue damage, nausea, cancer, and death in extreme cases [1–3]. There is a multitude of different types of materials that can be used as radiation shields, as they are versatile for different purposes [4–10]. For instance, concrete is typically used to line the walls in laboratories and nuclear power plants due to its low cost and its ability to be molded into many shapes [11]. However, concrete is prone to cracking over time and is not permeable to light [12]. To find a more efficient radiation shield, researchers have focused their attention on the development of glass as a radiation shield.

Glass offers the ability to manufacture a transparent shielding material has a low cost and is easily modifiable. By doping metal oxides into the glass, the radiation absorption properties of the material are improved. One of these oxides, TeO_2, can be used to form the glass network. TeO_2 is a glass intermediate, meaning that it can act as a glass former, creating the backbone of the glass network, or as a glass network modifier, altering the glass network. Tellurite glasses have desirable shielding properties such as low melting temperature and good chemical stability [13–15]. However, since

* Corresponding author. Ural Federal University, St. Mira, 19, 620002, Yekaterinburg, Russia.
E-mail address: mokhamed.khanfi@urfu.ru (M.Y. Hanfi).

the oxide is an intermediate, it is not very stable on its own due to its weak connectivity to the glass network. However, it can be vitrified, and by adding glass modifiers to the network, a more stable glass can be formed. Alkali oxides and alkaline earth oxides are commonly used as modifiers due to their ability to form non-bridging oxygens (NBOs) [14,16,17]. In this study, MgO is used to stabilize the glass network, as it increases the connectivity of the glass system by cross-linking NBOs. MgO also increases the chemical durability of the glasses, as well as the glass-forming ability of TeO_2, where the TeO_2 glasses have high density and high atomic number [18,19].

Simulations were used for this study, as even though experimentally determining the ability of a material to absorb incoming photons can be more valuable, constraints can often make this method less desirable. Experimental studies require the acquisition of metal oxides and radioisotopes to experiment, needing more time than simulations. Also, due to research facilities and universities being closed because of COVID-19, researchers resort to using alternative methods to conduct previously scheduled studies. In order to theoretically determine the radiation shielding properties of materials, programs such as Monte Carlo simulations are considered an efficient alternative to experimental procedures [20–23]. MCNP code was used to predict the average track length of the projected particle inside the shielding material [24]. Based on the average track length, the shielding materials such as mass attenuation coefficient (MAC) describes the ability for a material to attenuate or absorb the incoming photons, with a higher MAC signifying a more effective shield. To confirm the validity of the MCNP code as a valid way to determine the radiation shielding ability of the glasses, the XCOM database was also used to obtain the MACs of the glasses [25]. The two simulations were then compared to validate the data.

In addition to the radiation shielding ability of the glasses, their mechanical properties were also determined to figure out the strength and toughness of the glasses. Parameters such as the elastic modulus, a parameter that measures the material's resistance to being elastically deformed, of the glasses were investigated [26].

Overall, five magnesium tellurite glasses were theoretically investigated to evaluate their mechanical, and radiation shielding properties. The composition of each of the glasses was altered by increasing the weight% (wt%) of magnesium oxide in the glasses. The glasses were coded as TM10, TM20, TM30, TM40, and TM45 in increasing concentration of magnesium oxide content, and decreasing order of density.

2. Materials and methods

2.1. Mechanical properties

Mechanical moduli, such as Young's modulus (E), Bulk modulus (B), Shear modulus (S) and Longitudinal modulus (L), were calculated for five glass samples selected from Refs. [27]. The mechanical properties were calculated theoretically according to the Makishima–Mackenzie model [28–31]. The Makishima–Mackenzie model is based on the strength of the chemical bond between the glass compounds (dissociation energy G (kJ/cm^3)) and the packing factor (V$_i$) of the investigated glasses. The dissociation energy of the studied glasses can be determined according to equation (1).

$$G\left(kJ \Big/ cm^3\right) = \sum_i G_i x_i \tag{1}$$

where G_i and x_i refer to the dissociation energy and the molar weight fraction of ith constituent in the TM glasses.

The packing factor (V$_i$) for the investigated glasses is calculated based on the ionic radius of the constituent compounds and can be calculated through equation (2).

$$V_i\left(cm^3 \Big/ mol\right) = \frac{4\pi}{3} N_A\left(XR_A^3 + YR_o^3\right) \tag{2}$$

In the previous equation, N_A, R_A, R_o, X and Y represent Avogadro's number, the ionic radius of the metal, the ionic radius of oxygen, the number of metal atoms and the number of oxygen atoms, respectively. The packing density (V$_t$) is calculated based on the calculated V_i, molecular weight (M) and density (ρ) of the investigated glass as listed in equation (3).

$$V_t = \frac{\rho}{M} \sum_i V_i x_i \tag{3}$$

Furthermore, the elastic moduli are calculated according to the following equations:

$$E = 2V_t G \tag{4}$$

$$B = 1.2\, V_t E \tag{5}$$

$$S = \frac{3\, EB}{(9B - E)} \tag{6}$$

$$L = B + \frac{3}{4}\, S \tag{7}$$

$$\sigma = 0.5 - \frac{1}{7.2}V_t \tag{8}$$

$$H = \frac{(1 - 2\sigma)}{6(1 + \sigma)} \tag{9}$$

where σ and H represent Poisson's ratio and the micro-hardness of the investigated glasses.

2.2. Radiation shielding capacity

The gamma-ray shielding capacity of the TM glasses was investigated using Monte Carlo N-particle transport code (MCNP-5) [24]. To investigate the gamma-ray shielding properties, an input file containing all the information about the geometry, materials, sources, and detector was implemented and is illustrated in Fig. 1. The detector, glass samples and source were shielded from any outer interference by a lead cylinder with a thickness of 5 cm. The source was assumed to emit 10^6 photons per min along the +Z direction. In the present study, the selected sources are ^{60}Co with energies of 1.173 and 1.332 MeV, ^{137}Cs with an energy of 0.662 MeV and ^{152}Eu with energies of 0.344, 0.367, 0.411, 0.778, 0.963, 1.085, 1.111 and 1.406 MeV. The emitted photons were collimated using a lead collimator with a height of 10 cm, a diameter of 7 cm, and that possesses a central slit of 2 cm. After that, the collimated photons passed onto the TM glass, which was placed in the middle between the lead collimator and the detector. The chemical composition, density, and molar weight of the TM glasses were illustrated in Table 1. The detector was assumed to be an F4 tally to compute the average track length of the incoming photons in the TM glasses. Finally, the simulation runout and the output recorded that the relative error for the average track length measurement is less than 1% [32,33].

The linear attenuation coefficient (LAC, μ) is simulated based on the average track length recorded by MCNP-5. The LAC is the factor that predicts the ability of the studied material to attenuate and absorb the incoming photon energies. It can be described through the Lambert-Beer law [7].
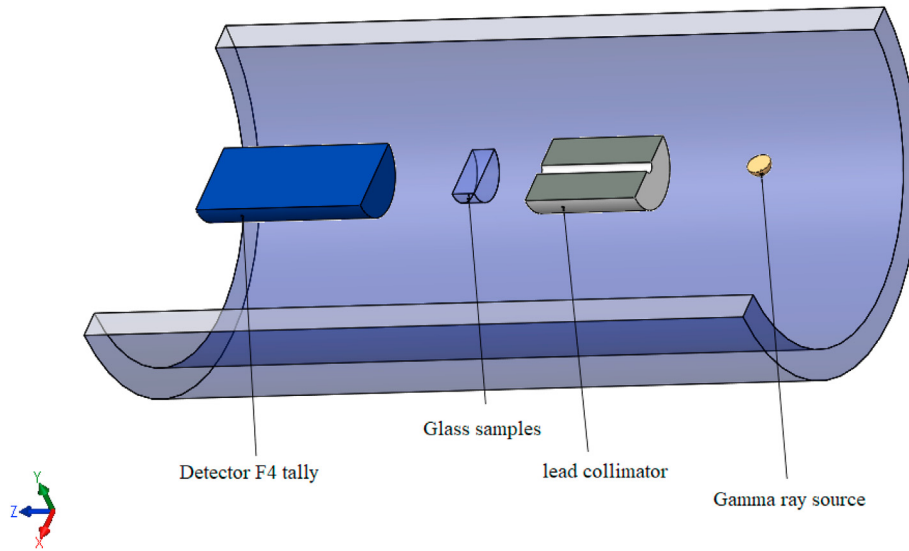
Fig. 1. The geometry setup of the simulation processes.

Table 1
The density and chemical composition of the studied glasses.

Glass code	The chemical composition (wt %)		Density (g/cm³)	Molecular weight (mol/g)	Molar volume (cm³/mol)
	TeO$_2$	MgO			
TM10	97.270	2.729	5.435	147.669	27.170
TM20	94.061	5.938	5.244	135.739	25.885
TM30	90.234	9.765	5.020	123.810	24.663
TM40	85.590	14.409	4.750	111.881	23.554
TM45	82.876	17.123	4.618	105.916	22.936

$$\mu\left(cm^{-1}\right) = \frac{1}{x} lnln\left(\frac{I_o}{I}\right) \tag{10}$$

The mass attenuation coefficient (MAC, μ_m) is used to predict the attenuation of the shielding material per unit density and can be calculated using equation (11) [34].

$$\mu_m = \frac{\mu\left(cm^{-1}\right)}{\rho\left(g\,cm^{-3}\right)} \text{ or } \mu_m = \sum_i w_i\left(\mu_m\right)_i \tag{11}$$

where I_o, I, x, ρ, w_i and $(\mu_m)_i$ represent the incoming intensity, transmitted intensity, glass thickness, glass density, fractional weight, and the mass attenuation coefficient of the ith constituent of the element, respectively.

The transmission factor (TF) is used to predict the ratio of gamma photons that can transmit a known thickness at any gamma photon energy and can be calculated using equation (12).

$$TF\left(\%\right) = \frac{I}{I_o} = expexp\left(-\mu x\right) \tag{12}$$

The half-value thickness (HVT, $\Delta_{0.5}$) is a shielding parameter that introduces the thickness of the shielding material that is able to diminish the incoming photon intensity to half of its starting value and can be calculated based on the LAC values according to equation (13) [35].

$$\Delta_{0.5} = \frac{lnln\left(2\right)}{\mu\left(cm^{-1}\right)} \tag{13}$$

Mean free path (MFP) is the parameter which calculates the average distance between two subsequent collisions. As the distance between the two following interactions (MFP) decreases, the number of interactions between the incoming photons and the atoms of the material increase; thus, absorbance and attenuation increase. MFP is similar to $\Delta_{0.5}$ in that it can be calculated based on the LAC values, as illustrated in equation (14).

$$MFP = \frac{1}{\mu\left(cm^{-1}\right)} \tag{14}$$

The program BXCOM was applied to calculate the values of the effective atomic number (Z_{eff}), equivalent atomic numbers (Z_{eq}) and the buildup factors (buildup factor (EBF) and energy absorption build-up factor (EABF)) [36]. The theoretical calculation was also used to calculate the effective fast neutron removal cross-section $\sum_R (cm^2 g^{-1})$. $\sum_R (cm^2 g^{-1})$ was calculated through equations (15) and (16) [37].

$$\sum_R\left(cm^2.g^{-1}\right) = 0.190\,Z^{-0.743} \quad (Z \leq 8) \tag{15}$$

$$\sum_R\left(cm^2.g^{-1}\right) = 0.125\,Z^{-0.565} \quad (Z > 8) \tag{16}$$

3. Results and discussion

3.1. The mechanical properties

It is known that TeO_2 is a good candidate for a glass former while MgO represents a glass modifier in the current study. The effect MgO oxides on the mechanical properties of the TeO_2 glasses was studied. To accomplish this, the mechanical moduli such as Young's modulus (Y), bulk's modulus (B), Shear modulus (S) and longitudinal modulus (L) were estimated theoretically using the Makishima−Mackenzie model. Fig. 2 depicts that the mechanical moduli gradually increase with the replacement of TeO_2 by MgO in the studied TM glasses. This increase can be related to the dissociation energy of both TeO_2 and MgO, where the dissociation energy for MgO is equal to 90 kJ/cm^3 while dissociation energy for TeO_2 is equal to 54 kJ/cm^3. The replacement of TeO_2 with MgO leads to an increase in the dissociation energy of the studied glasses. The dissociation energy for the studied TM glasses are equal to 57.600−70.200 kJ/cm^3 for TM10 glasses with 10 mol% MgO and TM45 glasses with 45 mol% of MgO, respectively. According to equations (1)–(9), the elastic (Young's) modulus is directly proportional to the dissociation energy. Thus, the elastic modulus increases gradually with the increase in the MgO content in the studied TM glasses. The elastic modulus was found to vary in the range between 59.317 and 70.428 GPa for glasses TM10 and TM 45 respectively [38].

The Bulk (B), Shear (S) and Longitudinal (L) moduli were calculated based on the estimated values of the elastic moduli and are directly proportional to the elastic modulus. Thus, the calculated values of the Bulk, Shear and Longitudinal moduli were found to gradually increase with the replacement of TeO_2 by MgO. The estimated values for the Bulk, Shear and Longitudinal moduli were listed in Table 2, where the Bulk's modulus increased from 36.651 to 42.394 GPa, the Shear modulus increased from 24.107 to 28.790 GPa and the longitudinal modulus increased from 68.794 to 80.781 GPa with the increase of MgO content from 10 to 45 mol% in the studied TM glasses.

Poisson's ratio (σ) and the microhardness were calculated for the studied glasses based on the estimated values of the mechanical moduli. Fig. 3 illustrated that Poisson's ratio decreased from 0.230 to 0.223 when replacing the TeO_2 content with MgO, while the microhardness (H) for the studied TM glasses gradually increased from 4.335 to 5.314 GPa with the increase in the MgO content from 10 to 45 mol % in the studied glasses.

3.2. Ionizing radiation shielding capacity

The linear attenuation coefficient (LAC) of the studied TM glasses was simulated using Monte Carlo N-particle transport code (MCNP-5). Fig. 4 depicts that the simulated LAC is affected by two factors. First, the incoming gamma photon energy (E). The highest LAC was obtained at low energies (for 0.343 MeV). The highest LAC decreased from 0.711 to 0.584 cm^{-1} for glasses TM10 and TM45, respectively. After that, the simulated LAC values gradually decreased with the increase in the incoming gamma photon energy. The observed decrease is related to the Compton scattering interaction (CS), where its cross-section is inversely proportional to the incoming energy ($\sigma_{com} \propto E^{-1}$). The lowest LAC obtained at a gamma photon energy of 1.406 MeV and decreased from 0.259 to 0.223 cm^{-1} for glasses TM10 and TM45, respectively [39,40].

Secondly, the chemical composition of the investigated glasses. The insertion of MgO content on TeO_2 glasses reduces the molecular weight of TM glasses. Hence, Z_{eff} falls gradually by decreasing the molecular weight of the TM glasses. The LAC reaches the
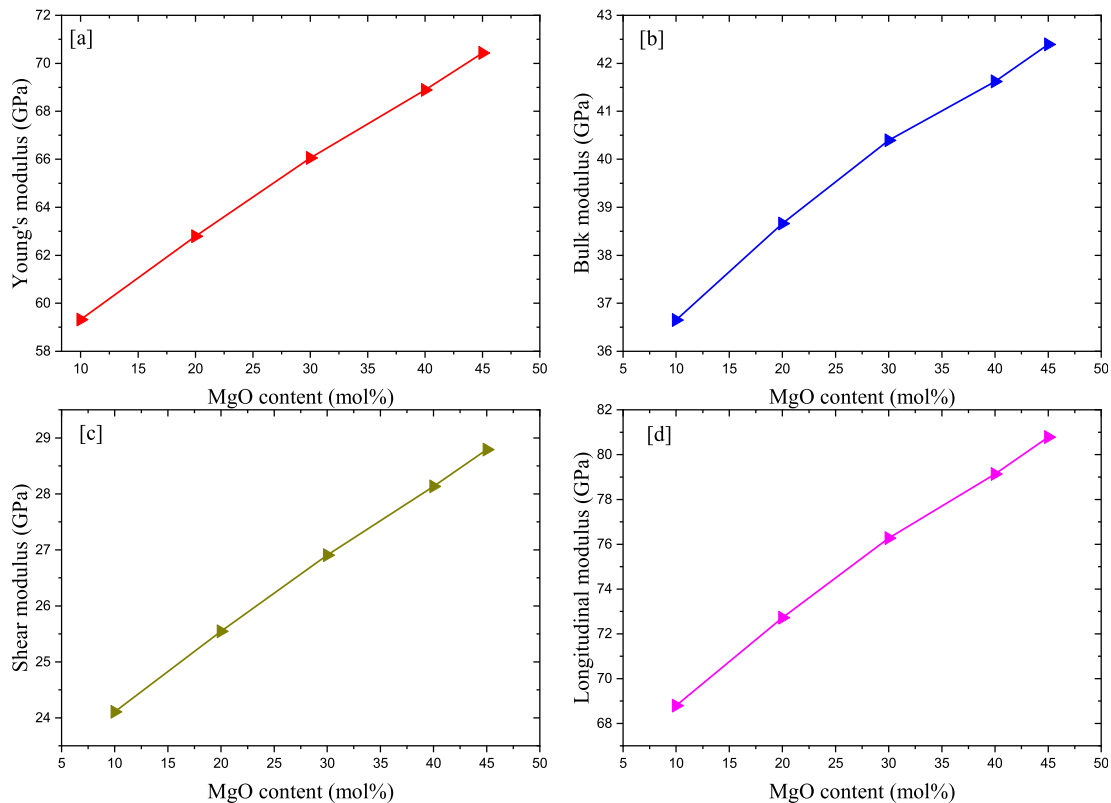

Fig. 2. Variation of the elastic moduli as a function of the MgO contents.

Table 2
The mechanical parameters and elastic moduli of the studied glasses.

| Glass code	V_i cm^3/mol	G kJ/cm^3	V_t cm^3/mol	Y (GPa)	B (GPa)	S (GPa)	σ	H (GPa)	L (GPa)	V_l (m/sec)	V_s (m/sec)
TM10	13.990	57.600	0.515	59.317	36.651	24.107	0.230	4.335	68.794	3557.761	2106.085
TM20	13.280	61.200	0.513	62.796	38.661	25.542	0.229	4.610	72.716	3723.788	2206.962
TM30	12.570	64.800	0.510	66.052	40.397	26.905	0.227	4.888	76.271	3897.872	2315.090
TM40	11.860	68.400	0.504	68.882	41.621	28.134	0.224	5.174	79.133	4081.623	2433.726
TM45	11.505	70.200	0.502	70.428	42.394	28.790	0.223	5.314	80.781	4182.418	2496.869
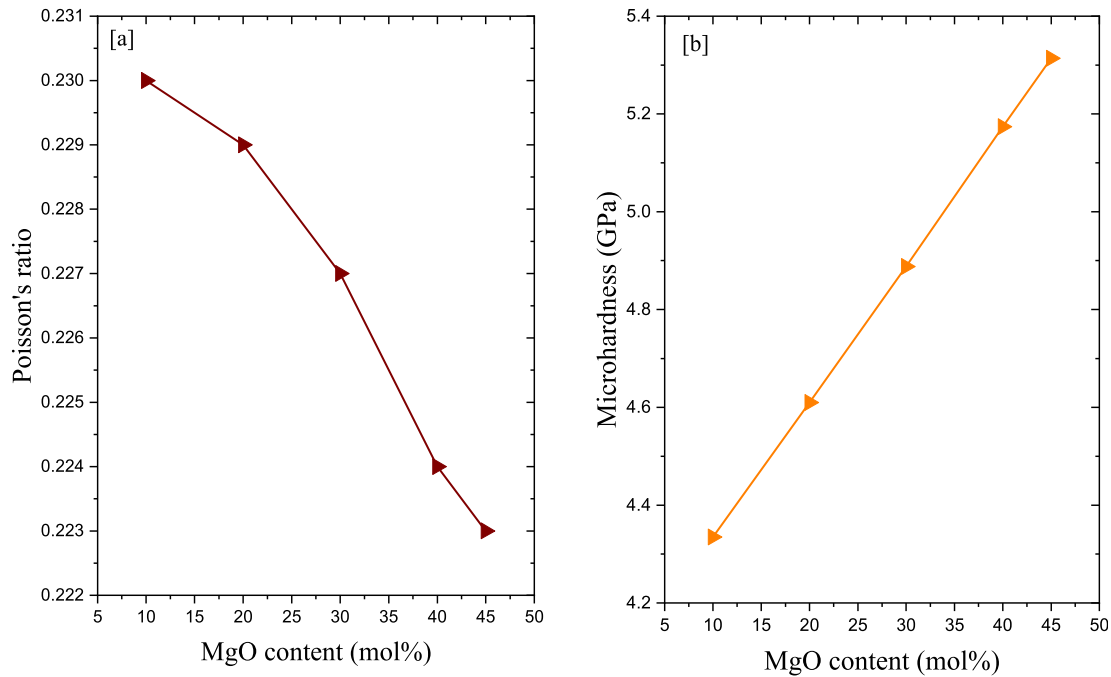
Fig. 3. Variation of the Poisson's ratio and microhardness versus the MgO contents.

maximum for TM10 with 10 mol% MgO, while it drops to lower values for the TM45 glass with 45 mol% MgO. The TM10 glass was observed to have higher LAC values than TM20, TM30, TM40 and TM45. The LAC values for TM 10 decreased from 0.711 to 0.259 cm^{-1}, while decreasing from 0.584 to 0.223 cm-1 for the TM45 glass at gamma photon energies between 0.343 and 1.406 MeV. The LAC is observed to slowly decrease with the addition of MgO content to the TeO$_2$ glasses. This decrease is due to the CS cross-section, which is directly proportional to the Z_{eff} (σ_{com} α Z_{eff}).

The MAC is calculated based on the simulated data of the LAC for the investigated TM glasses. Moreover, the MAC for the TM glasses is theoretically calculated using the XCOM database. The difference (%) between the simulated MAC and the calculated MAC is calculated through equation (17) and is listed in Table 3. The diff (%) was observed to be less than 2% for all investigated TM glasses.

$$Diff\ (\%) = \frac{\left[(\mu_m)_{mcnp} - (\mu_m)_{xcom}\right]}{(\mu_m)_{mcnp}} \times 100 \qquad (17)$$

Fig. 5 illustrates the variation of the TF of the investigated glass versus the glass thickness at some fixed photon energies (0.367, 0.662, 1.173 and 1.406 MeV). The TF was affected by two significant factors. First, the TF was observed to vary linearly with the incoming photon energy. At a low energy of 0.367 MeV, the TF had the lowest values and decreased from 0.517 to 0.037 for the TM10 glass, while the highest TF values decreased from 0.580 to 0.065 for

the TM45 glass. Furthermore, at a high energy of 1.406 MeV, the TF for theTM10 glass was observed to decrease from 0.772 to 0.274, while diminishing from 0.800 to 0.327 for the TM45 glass. Increasing the incoming photon energy leads to a decrease of the gamma photon wavelength (E = hc/λ), which increases the penetration power of the incoming photons. Thus, the number of photon interactions inside the TM glasses decreased when energy increases, so the TF of the incident photons increased. Second, it was found that the TF decreased with increasing glass thickness. The TF was found to decrease from 0.517 to 0.037 for thicknesses of 1 and 5 cm, respectively, for the TM10 glass at 0.367 MeV. When increasing the glass thickness, the time required for photons to pass through the glass thickness also increases. Thus, more photon interactions inside the glass material will occur and the number of photons transmitted through the material will decrease.

Fig. 6 demonstrates that $\Delta_{0.5}$ has an inverse correlation with the LAC according to Eq (13). For various energies, $\Delta_{0.5}$ is slowly increased when increasing the energy of the incoming photons. The $\Delta_{0.5}$ of the TM10 glasses increased from 0.975 to 2.681 cm, while it increased from 1.187 to 3.102 cm for TM45 at photon energies between 0.367 and 1.406 MeV. It was observed that the CS interaction is predominant in the selected range of energy (0.365−1.406 MeV), so $\Delta_{0.5}$ α E. Consequently, $\Delta_{0.5}$ was found to increase with photon energy.

The MgO content has a significant effect on the simulated $\Delta_{0.5}$ as illustrated in Fig. 6. It is observed that the insertion of MgO content gradually increased $\Delta_{0.5}$. The $\Delta_{0.5}$ increased from 0.975 to 1.187 cm
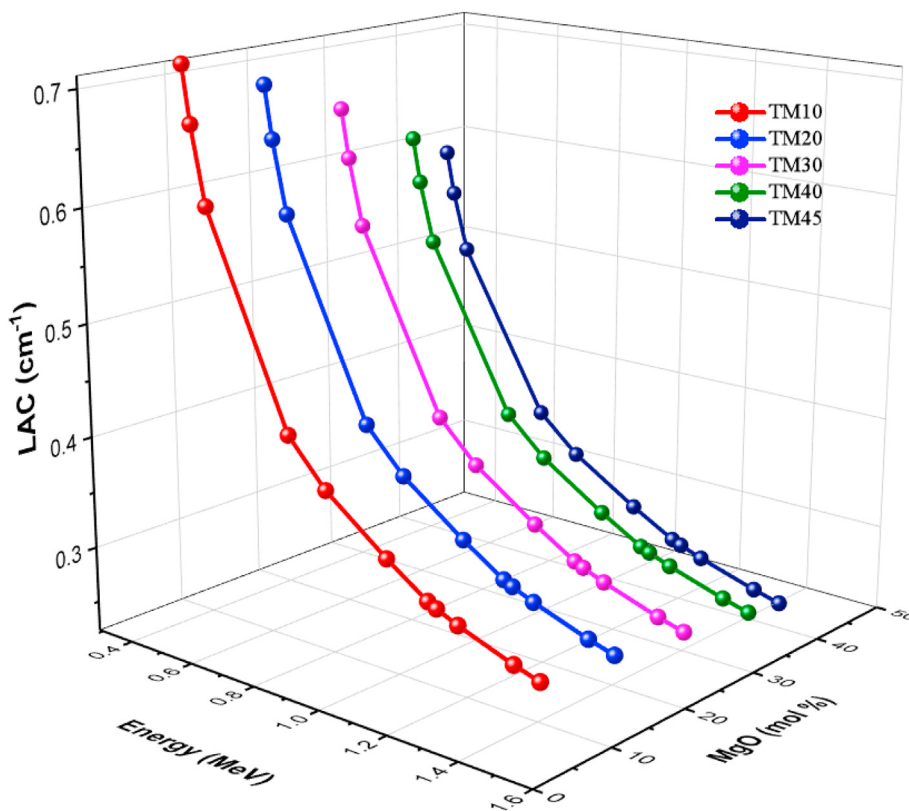
Fig. 4. Variation of the LAC of the studied glasses versus the incident gamma ray energy at various dropping contents.

Table 3
Comparison between the simulated and calculated Mass attenuation coefficient, MAC (cm^2 g^{-1}).

Energy (MeV)	MAC (cm^2 g^{-1})														
	TM10			TM20			TM30			TM40			TM45		
	MCNP	XCOM	diff (%)	MCNP	XCOM	diff (%)	MCNP	XCOM	diff (%)	MCNP	XCOM	diff (%)	MCNP	XCOM	diff (%)
0.344	0.131	0.131	0.026	0.130	0.130	0.037	0.129	0.129	0.012	0.127	0.127	0.031	0.126	0.126	0.027
0.367	0.122	0.122	0.224	0.121	0.121	0.274	0.120	0.120	0.202	0.119	0.119	0.208	0.118	0.118	0.245
0.411	0.109	0.109	0.154	0.108	0.109	0.139	0.108	0.108	0.120	0.107	0.107	0.124	0.107	0.107	0.130
0.662	0.075	0.075	0.306	0.075	0.075	0.294	0.075	0.075	0.292	0.075	0.075	0.283	0.075	0.075	0.273
0.778	0.068	0.068	0.256	0.068	0.068	0.256	0.068	0.068	0.247	0.068	0.068	0.241	0.068	0.068	0.237
0.963	0.059	0.060	0.238	0.060	0.060	0.235	0.060	0.060	0.241	0.060	0.060	0.232	0.060	0.060	0.234
1.085	0.055	0.056	1.760	0.055	0.056	1.701	0.055	0.056	1.627	0.055	0.056	1.553	0.055	0.056	1.564
1.111	0.054	0.055	1.758	0.054	0.055	1.700	0.054	0.055	1.643	0.055	0.055	1.568	0.055	0.056	1.511
1.173	0.052	0.053	1.629	0.052	0.053	1.589	0.053	0.054	1.533	0.053	0.054	1.459	0.053	0.054	1.421
1.332	0.049	0.050	1.357	0.049	0.050	1.315	0.049	0.050	1.260	0.050	0.050	1.206	0.050	0.050	1.183
1.406	0.048	0.048	1.268	0.048	0.048	1.239	0.048	0.049	1.195	0.048	0.049	1.141	0.048	0.049	1.107

for TM10 and TM45 glasses, respectively. With the addition of MgO content to the tellurite glasses, the molecular weight and density of the investigated glasses decreased. Moreover, the Z_{eff} of the TM glasses decreases, which leads to a decrease to the LAC and an increase to the $\Delta_{0.5}$ of the TM glasses.

Fig. 7 shows the variation of Z_{eff} against the gamma photon energy and MgO contents. According to the gamma energy range 0.015–15 MeV, three different interactions were observed. The first is the photoelectric effect (PE), which appears at low energies, between 0.015 and 0.1 MeV. The estimated values of Z_{eff} were observed to speedily drop with the increase of photon energy in this range. This drop was found as a result of the PE cross-section, where $\sigma_{PE} \propto E^{-3.5}$. An unexpected increase in the Z_{eff} values was obtained at a photon energy 0.0318 MeV due to the X-ray K-absorption edges of Te [33]. After that, above 0.1 MeV, where CS is

prevalent, the estimated values for Z_{eff} were found to reduce moderately with an increase in the photon energy. This observation is due to the CS cross-section where $\sigma_{CS} \propto E^{-1}$. Above several MeV, the Z_{eff} began to increase with the increase in photon energy. It is related to the pair production cross-section where $\sigma_{PP} \propto \log E$.

Unlike Z_{eff}, Z_{eq} was calculated based on MAC$_{CS}$. Fig. 8 shows the variation of Z_{eq} with photon energy, where the lower values of Z_{eq} were estimated for the PE region (0.015–0.1 MeV). Above 0.1 MeV, the Z_{eq} increased gradually with increasing photon energy. The highest value of Z_{eq} was achieved around 1 MeV, where the main interaction is CS. Z_{eq} moderately decreases with an increase in the PP interactions.

To describe the ability of the material to remove or accumulate incoming photons, the BXCOM program was applied to calculate the buildup factors EBF and EABF for the studied glasses. Figs. 9 and
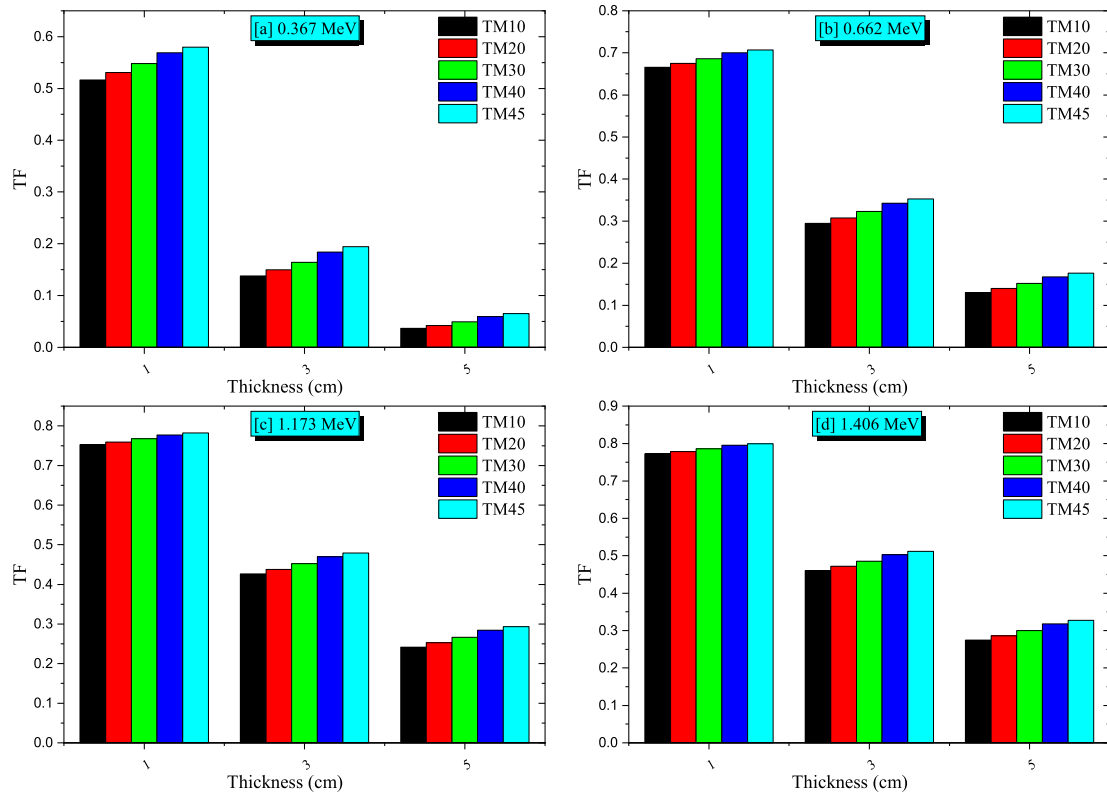
Fig. 5. The transmission rate of the incoming gamma photons as a function of the glass thickness at some fixed gamma photon energies.
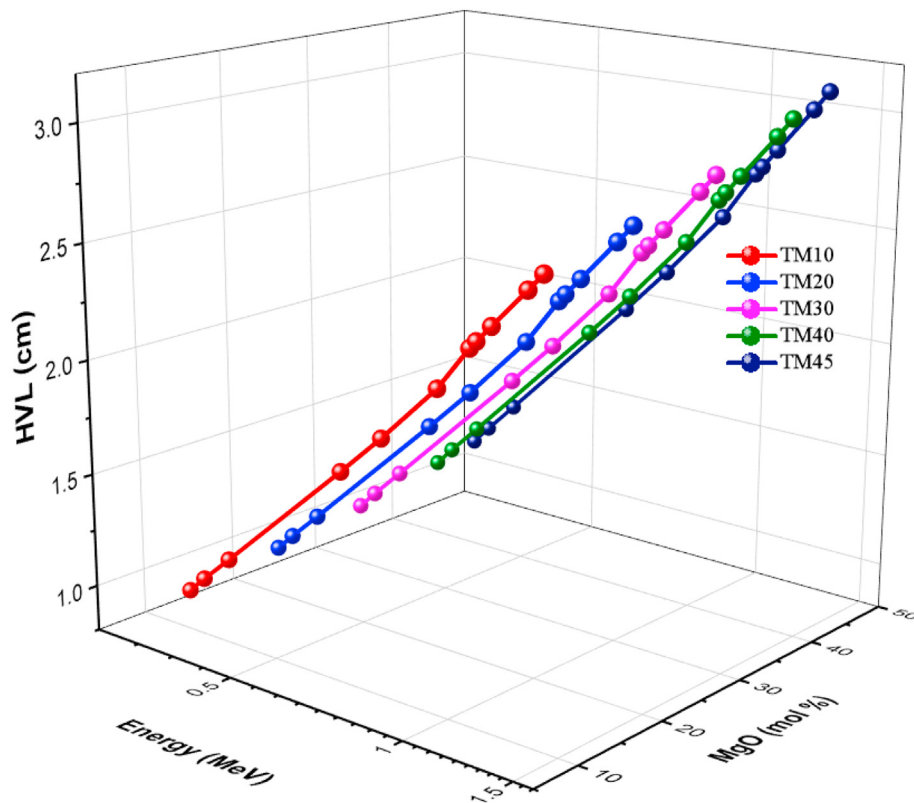

Fig. 6. Variation of the half value thickness ($\Delta_{0.5}$) of the fabricated glasses as a function of incoming gamma photon energy and MgO contents.
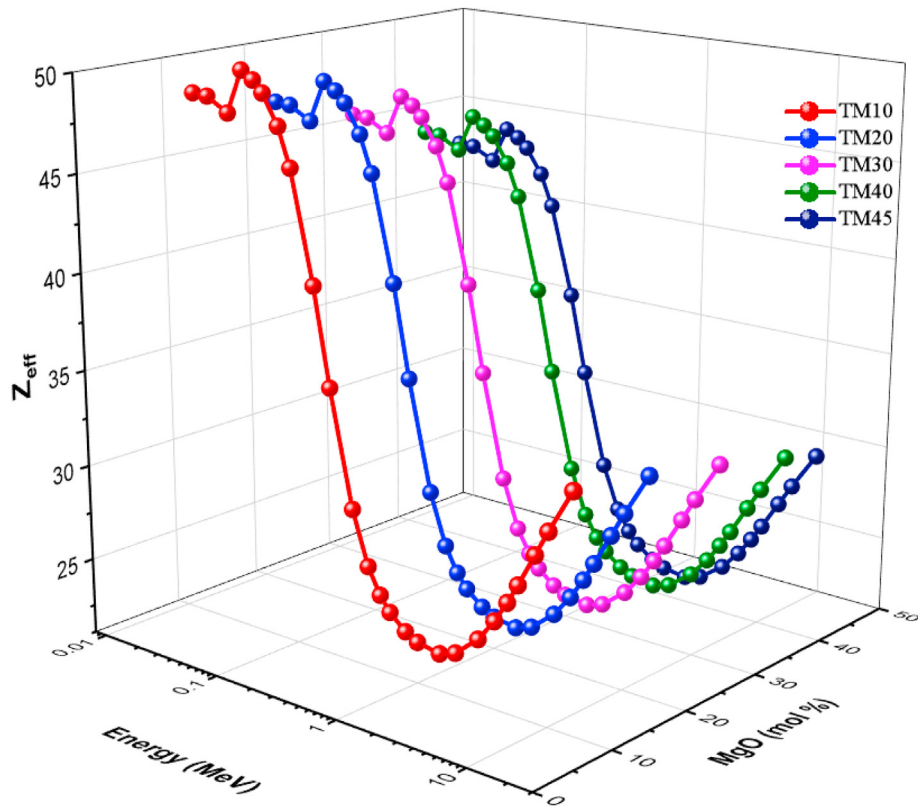
Fig. 7. Variation of the effective atomic number of the studied glasses as a function of the incoming photon energies and the MgO content.
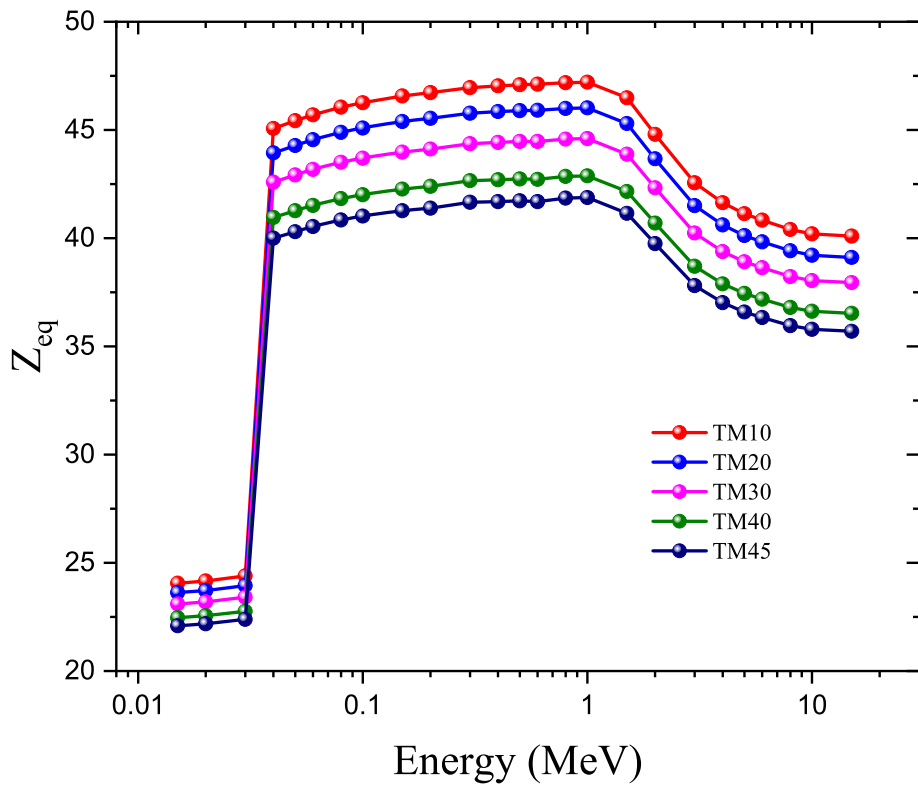

Fig. 8. Variation of the equivalent atomic number of the studied glasses as a function of the incoming photon energy and the MgO content.
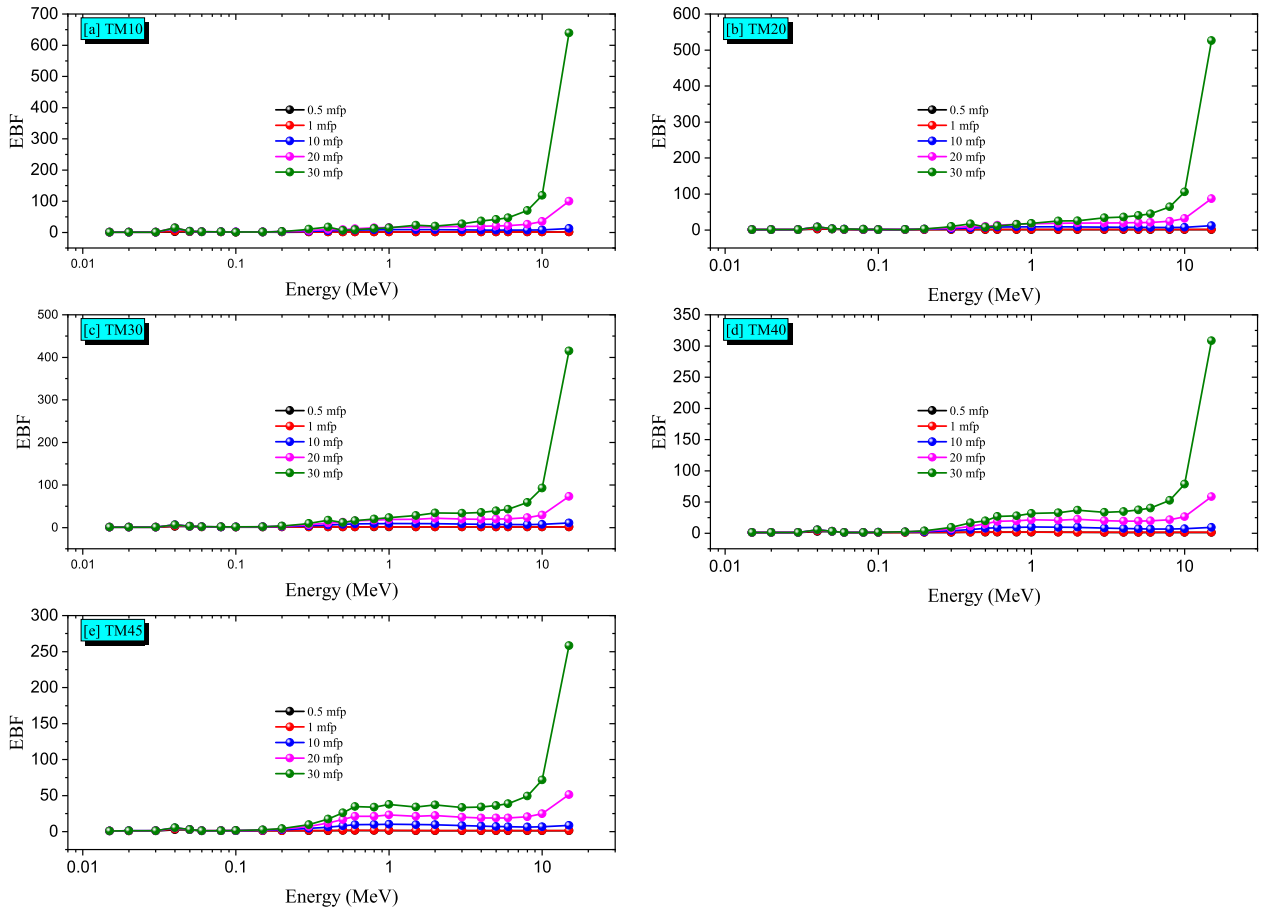
Fig. 9. The variation of the exposure buildup factor as a function of the incoming gamma photon energies at some fixed penetration depths.

10 depict the variation of the EBF and EABF as a function of the incoming photon energy and the penetration depth (PD). Two parameters were found to have a significant effect on the calculated values of EBF and EABF. Incoming photon energy represents the first factor where the accumulation of photons inside the shielding materials affected the photon interaction type. For low gamma-ray energy where the PE interaction is the main interaction, the calculated values of EBF and EABF were very low. The reason for this is due to the PE interaction depleting the photon energy to eject a boundary electron. With the increase in the photon energy above 0.1 MeV, CS began to increase while the PE decreased. Thus, the estimated values of EBF and EABF were observed to increase with the increase the incoming energy. The CS interaction exhausted a part of the photon energy to expel one boundary electron, but the photon is still in the shielding material. Thus, the number of photons that accumulate inside of the material increases. At 1 MeV, the CS interaction reaches its maximum and the accumulation of photons possesses the highest values for all investigated glasses. The PP interaction begins to increase gradually above 1 MeV. Thus, a very small decrease in EBF and EABF was detected. After reaching very high energies (E > 10 MeV), a high increase in EBF and EABF can be detected, especially at high PD (PD > 20 mfp).

The chemical composition of the investigated TM glasses is the second parameter that effects the estimated values of EBF and EABF. According to the data presented in Figs. 9 and 10, the calculated values of EBF and EBF decrease gradually with the replacement of TeO$_2$ with MgO content. The TM10 glass TM10 was observed to possess the highest EBF and EABF at the energy range between 0.015 and 15 MeV. After that, the values of EBF and EABF decrease

gradually with the increase in the MgO content in the investigated TM glasses, following the pattern (EBF)$_{TM10}$ > (EBF)$_{TM20}$ > (EBF)$_{TM30}$ > (EBF)$_{TM40}$ > (EBF)$_{TM45}$ and (EABF)$_{TM10}$ > (EABF)$_{TM20}$ > (EABF)$_{TM30}$ > (EABF)$_{TM40}$ > (EABF)$_{TM45}$. It is known that the accumulation of photons in the case of heavy compounds such as TeO$_2$ is higher than the accumulation of photons for light compounds such as MgO. Thus, the replacement of TeO$_2$ by MgO leads to decreasing the accumulation of photons inside the investigated glasses.

Fig. 11 displays the variation of the effective removal cross-section (ERCSFN) $\sum_R$ (cm^2 g^{-1}) of the fast neutrons for the investigated TM glasses. In the present work, the ERCSFN was estimated using Eqs (15) and (16). The estimated results showed that the TM10 glass with the lowest MgO ratio (MgO = 10 mol%) possesses the lowest ERCSFN ($\sum_R$ = 0.0193 cm^2 g^{-1}), while TM45 with the highest MgO content (MgO = 45 mol%) possesses the highest ERCSFN ($\sum_R$ = 0.0215 cm^2 g^{-1}) among the investigated TM glasses. It is observed that the ERCSFN gradually increased with the increase in the insertion ratio of MgO in the studied glasses. This trend is due to the replacement of TeO$_2$, which has a higher molecular weight (MW = 159.60 g mol^{-1}) and effective atomic number, by MgO, which has a lower molecular weight (MW = 40.30 g mol^{-1}) and effective atomic number.

4. Conclusion

The mechanical moduli were calculated based on the Makishima–Mackenzie model for five glasses composed of TeO$_2$ and MgO. Young's modulus was found to increase from 59.31 to 70.42 GPa with an increase in the MgO content from 10 to 45 mol %
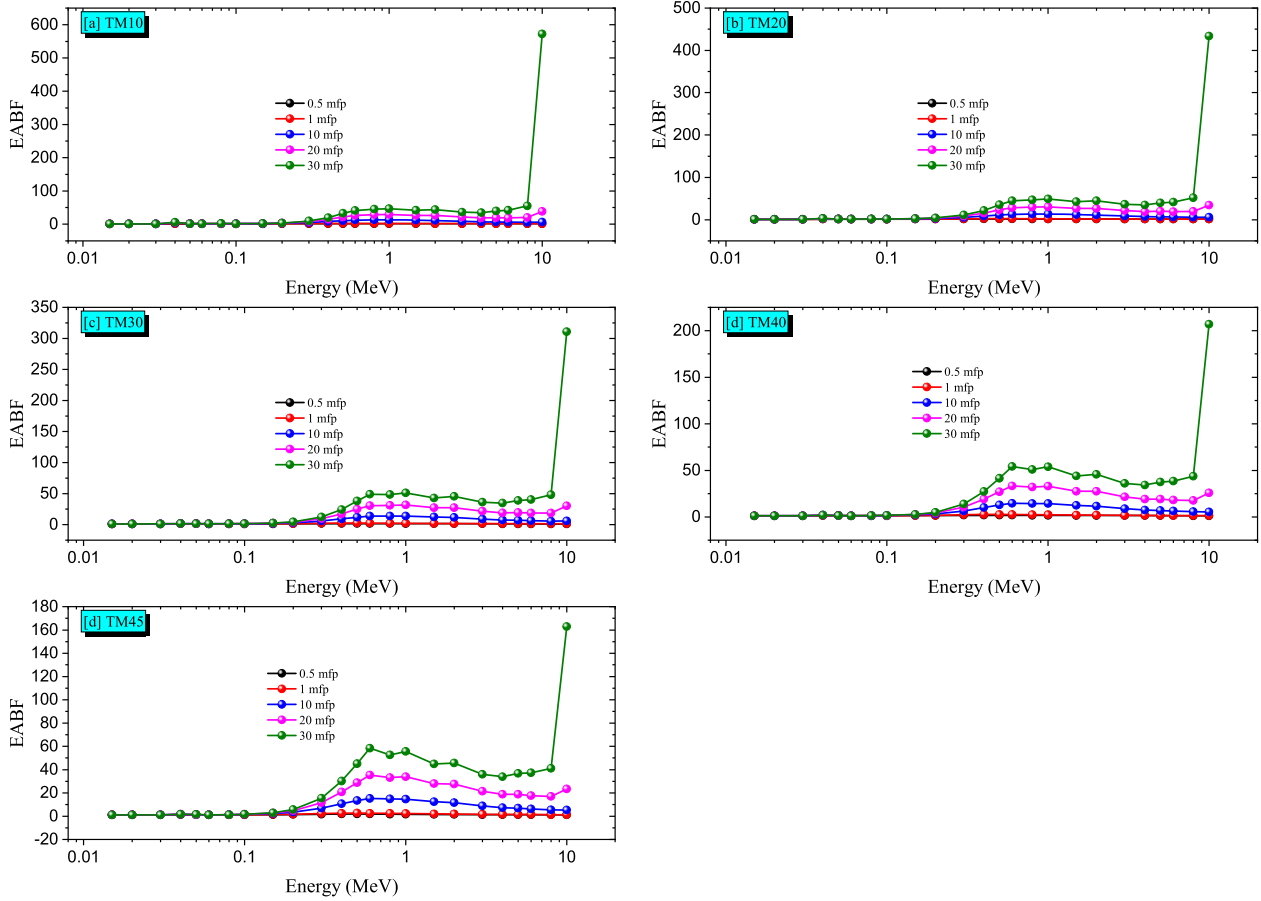
Fig. 10. The Variation of the energy absorption buildup factor (EABF) as a function of the incoming gamma photon energy at some fixed penetration depths.
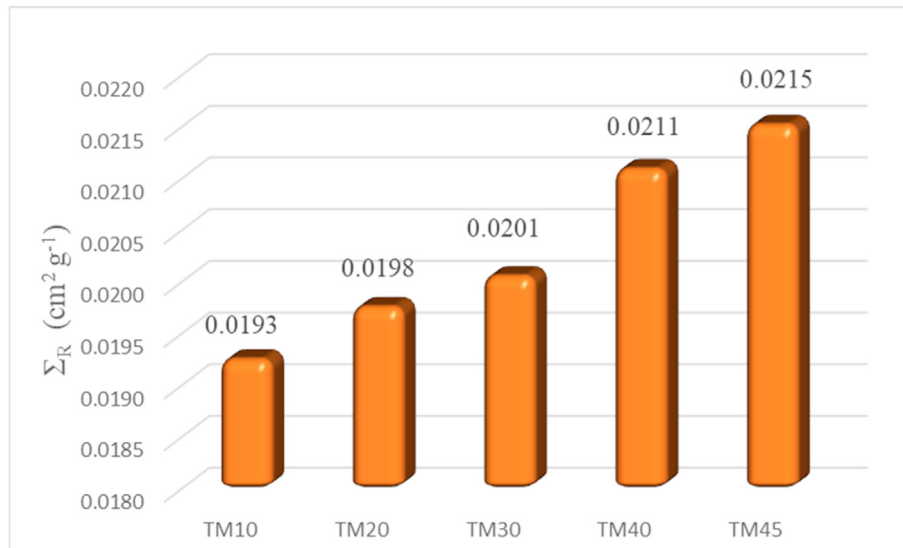

Fig. 11. The fast neutron effective removal cross section for the studied TM glasses.

respectively. Similar to the Young's modulus, Bulk, Shear and Longitudinal moduli were found to increase with the increase of MgO content in the investigated glasses. On the other hand, Poisson's ratio and packing density were found to reduce in the range between 0.230–0.223 and 0.515–0.502 with the increase in the MgO content between 10 and 45 mol% respectively. Thus, replacing TeO$_2$ with MgO was found to enhance the mechanical properties of the investigated glasses. The Monte Carlo N particle transport code (MCNP-5) was used to simulate gamma photon shielding parameters. The simulated data depicts that gamma ray shielding

parameters such as LAC, MAC, TF and $\Delta_{0.5} \alpha E$ decreased with the increase of the MgO content in the investigated glasses. The highest LAC was achieved by the TM10 glasses and varied in the range of $0.0259-0.711$ cm^{-1}, while the lowest LAC was obtained for TM45 glasses and varied in the range $0.223-0.587$ cm^{-1} for gamma photons between 0.344 and 1.406 MeV. The BXCOM program was used to estimate the buildup factors for the glasses. The calculated values showed that EBF and EABF were gradually enhanced with the increase of the MgO contents in the TM glasses. Finally, the effective removal cross section ($\sum_R$) was calculated and the results showed that the lowest $\sum_R$ was achieved by TM10 and was equal to 0.0193 cm^2 g^{-1}, while the highest $\sum_R$ was achieved for TM45 and was equal to 0.0215 cm^2 g^{-1}.

Declaration of competing interest

The authors declare that they have no known competing financial interests or personal relationships that could have appeared to influence the work reported in this paper.

References

[1] H.O. Tekin, Shams A.M. Issa, K.A. Mahmoud, F.I. El-Agawany, Y.S. Rammah, G. Susoy, M.S. Al-Buriahi, Mohamed M. Abuzaid, I. Akkurt, Nuclear radiation shielding competences of Barium (Ba) reinforced borosilicate glasses, Emerg. Mater. Res. 9–4 (2020), https://doi.org/10.1680/jemmr.20.00185.

[2] Yonca Yahşi Çelen, Atilla Evcin, Synthesis and characterizations of magnetite–borogypsum for radiation shielding, Emerg. Mater. Res. 9–3 (2020) 770–775, https://doi.org/10.1680/jemmr.20.00098.

[3] Feride Kulali, Simulation studies on the radiological parameters of marble concrete, Emerg. Mater. Res. (2020), https://doi.org/10.1680/jemmr.20.00307, 9-4.

[4] S.S. Obaid, M.I. Sayyed, D.K. Gaikwad, P.P. Pawar, Attenuation coefficients and exposure buildup factor of some rocks for gamma ray shielding applications, Radiat. Phys. Chem. 148 (2018) 86–94.

[5] S.S. Obaid, M.I. Sayyed, D.K. Gaikwad, H.O. Tekin, Y. Elmahroug, P.P. Pawar, Photon attenuation coefficients of different rock samples using MCNPX, Geant4 simulation codes and experimental results: a comparison study, Radiat. Eff. Defect Solid 173 (2018) 900–914, https://doi.org/10.1080/10420150.2018.1505890.

[6] D.K. Gaikwad, M.I. Sayyed, S.N. Botewad, S.S. Obaid, Z.Y. Khattari, U.P. Gawai, F. Afaneh, M.D. Shirsat, P.P. Pawar, Physical, structural, optical investigation and shielding features of tungsten bismuth tellurite-based glasses, J. Non-Cryst. Solids 503–504 (2019) 158–168.

[7] S.S. Obaid, D.K. Gaikwad, P.P. Pawar, Determination of gamma ray shielding parameters of rocks and concrete, Radiat. Phys. Chem. 144 (2018) 356–360.

[8] Iskender Akkurt, Effective atomic and electron numbers of some steels at different energies, Ann. Nucl. Energy 36–11 (12) (2009) 1702–1705, https://doi.org/10.1016/j.anucene.2009.09.005.

[9] Yasser Saad Rammah, Ashok Kumar, Karem Abdel-Azeem Mahmoud, Raouf El-Mallawany, Fouad Ismail El-Agawany, Gulfem Susoy, Huseyin Ozan Tekin, SnO-reinforced silicate glasses and utilization in gamma-radiation-shielding applications, Emerg. Mater. Res. 9–3 (2020) 1000–1008, https://doi.org/10.1680/jemmr.20.00150.

[10] Roya Boodaghi Malidarrea, Feride Kulali, Aysun Inal, Oz Ali, Monte Carlo simulation of the Waste Soda-Lime-Silica Glass system contained Sb₂O₃, Emerg. Mater. Res. (2020), https://doi.org/10.1680/jemmr.20.00202, 9-4.

[11] K.A. Mahmoud, O.L. Tashlykov, A.F. El Wakil, H.M.H. Zakaly, I.E. El Aassy, Investigation of radiation shielding properties for some building materials reinforced by basalt powder, AIP Conf. Proc. (2019) 2174.

[12] A.S. Abouhaswa, M.I. Sayyed, A.S. Altowyan, Y. Al-Hadeethi, K.A. Mahmoud, Synthesis, structural, optical and radiation shielding features of tungsten tri-oxides doped borate glasses using Monte Carlo simulation and phy-X program, J. Non-Cryst. Solids 543 (2020) 120134, https://doi.org/10.1016/j.jnoncrysol.2020.120134.

[13] Y. Al-Hadeethi, M.I. Sayyed, A comprehensive study on the effect of TeO₂ on the radiation shielding properties of TeO₂–B₂O₃–Bi₂O₃–LiF–SrCl₂ glass system using Phy-X/PSD software, Ceram. Int. 46 (2020) 6136–6140.

[14] Y. Al-Hadeethi, M.I. Sayyed, Hiba Mohammed, Lia Rimondin, X-ray photons attenuation characteristics for two tellurite based glass systems at dental diagnostic energies, Ceram. Int. 46 (2020) 251–257.

[15] M.I. Sayyed, R. El-mallawany, Shielding properties of (100-x)TeO₂e(x)MoO₃ glasses, Mater. Chem. Phys. 201 (2017) 50–56.

[16] Y.S. Rammah, F.I. El-Agawany, K.A. Mahmoud, A. Novatski, R. El-Mallawany, Role of ZnO on TeO₂.Li₂O.ZnO glasses for optical and nuclear radiation shielding applications utilizing MCNP5 simulations and WINXCOM program, J. Non-Cryst. Solids 544 (2020) 120162, https://doi.org/10.1016/j.jnoncrysol.2020.120162.

[17] N.S. Hussain, G. Hubgerford, R. El-mallawany, M.J.M. Gomes, M.A. Lopes, N. Ali, J.D. Santos, S. Buddhudu, Absorption and emission analysis of RE³⁺(Sm³⁺and Dy³⁺): lithium boto tellurite glasses, J. Nanosci. Nanotechnol. 9 (2009) 3672–3677.

[18] V. Kozhukharov, M. Marinov, G. Grigorova, Glass-formation range in binary tellurite systems containing transition metal oxides, J. Non-Cryst. Solids 28 (1978) 429–430.

[19] H. Bürger, K. Kneipp, H. Hobert, W. Vogel, V. Kozhukharov, S. Neov, Glass formation, properties and structure of glasses in the TeO₂ZnO system, J. Non-Cryst. Solids 151 (1992) 134–142.

[20] K.A. Mahmoud, E. Lacomme, M.I. Sayyed, Ö.F. Özpolat, O.L. Tashlykov, Investigation of the gamma ray shielding properties for polyvinyl chloride reinforced with chalcocite and hematite minerals, Heliyon 6 (2020), e03560.

[21] A.S. Abouhaswa, M.I. Sayyed, Y. Al-Hadeethi, A.S. Altowyan, K.A. Mahmoud, Evaluation of optical and gamma ray shielding features for tungsten-based bismuth borate glasses, Opt. Mater. 106 (2020) 109981, https://doi.org/10.1016/j.optmat.2020.109981.

[22] F.I. El-Agawany, O.L. Tashlykov, K.A. Mahmoud, Y.S. Rammah, The radiation-shielding properties of ternary SiO₂–SnO–SnF₂ glasses: simulation and theoretical study, Ceram. Int. (2020), https://doi.org/10.1016/j.ceramint.2020.04.042.

[23] Y.S. Rammah, K.A. Mahmoud, E. Kavaz, A. Kumar, F.I. El-Agawany, The role of PbO/Bi₂O₃ insertion on the shielding characteristics of novel borate glasses, Ceram. Int. (2020), https://doi.org/10.1016/j.ceramint.2020.04.018.

[24] X-5 Monte Carlo Team, MCNP-A General Monte Carlo N-Particle Transport Code, Version 5, Los Alamos Controlled Publication, 2003. LA-CP-03-0245.

[25] M.J. Berger, j H. Hubbel, XCOM: Photon Cross Sections Database, 1987. Gaithersburg, MD 20899, USA, http://physics.nist.gov/xcom.

[26] A. El-Adawy, R. El-Mallawany, Elastic modulus of tellurite glasses, J. Mater. Sci. Lett. 5 (1996) 2065–2067.

[27] H. Elkholy, H. Othman, I. Hager, M. Ibrahim, D. de Ligny, Thermal and optical properties of binary magnesium tellurite glasses and their link to the glass structure, J. Alloys Compd. (2020), https://doi.org/10.1016/j.jallcom.2020.153781.

[28] A. Makishima, J.D. Mackenzie, Direct calculation of Young's modulus of glass, J. Non-Cryst. Solids 12 (1973) 35–45.

[29] A. Makishima, J.D. Mackenzie, Calculation of Bulks modulus, Shear modulus and Piosson's ratio of glass, J. Non-Cryst. Solids 17 (1975) 147–157.

[30] S. Inaba, S. Fujino, K. Morinaga, Young's modulus and compositional parameters of oxide glasses, J. Am. Ceram. Soc. 82 (1999) 3501–3507.

[31] A. Abd El-Moneim, H.Y. Alfifi, Approach to dissociation energy and elastic properties of vanadate and V₂O₅-contained glasses from single bond strength: Part I, Mater. Chem. Phys. 207 (2018) 271–281, https://doi.org/10.1016/j.matchemphys.2017.12.057.

[32] R. Divina, K. Marimuthu, K.A. Mahmoud, M.I. Sayyed, Physical and structural effect of modifiers on dysprosium ions incorporated boro-tellurite glasses for radiation shielding purposes, Ceram. Int. (2020), https://doi.org/10.1016/j.ceramint.2020.04.102.

[33] M.I. Sayyed, M.H.M. Zaid, N. Effendy, K.A. Matori, H.A. Sidek, E. Lacomme, K.A. Mahmoud, M.M. AlShammari, The influence of PbO and Bi₂O₃ on the radiation shielding and elastic features for different glasses, J. mater. Res. Technol. 9 (2020) 8429–8438, https://doi.org/10.1016/j.jmrt.2020.05.113.

[34] Y. Al-Hadeethi, M.I. Sayyed, Y.S. Rammah, Fabrication, optical, structural and gamma radiation shielding characterizations of GeO₂-PbO-Al₂O₃–CaO glasses, Ceram. Int. 46 (2020) 2055–2062.

[35] Qiuling Chen, K.A. Naseer, K. Marimuthu, P. Suthanthira Kumar, Baoji Miao, K.A. Mahmoud, M.I. Sayyed, Influence of modifier oxide on the structural and radiation shielding features of Sm3+-doped calcium telluro-fluoroborate glass systems, J. Austr. Ceram. Soc. (2020), https://doi.org/10.1007/s41779-020-00531-8.

[36] Ö. Eyecioğlu, A.M. El-Khayatt, Y. Karabul, M. Çağlar, O. Toker, O. İçelli, BXCOM: a software for computation of radiation sensing, Radiat. Eff. Defect Solid 174 (2019) 506–518, https://doi.org/10.1080/10420150.2019.1606811.

[37] A. El Abd, G. Mesbah, N.M.A. Mohammed, A. Ellithi, A simple Method for determining the effective removal cross section for fast neutrons, J. Radiat. Nucl. Appl. 2 (2016) 53–85.

[38] A. Abd El-Moneim, R. El-Mallawany, Analysis and prediction for elastic properties of quaternary tellurite Ag₂O–V₂O₅–MoO₃–TeO₂ and WO₃–B₂O₃–MgO–TeO₂ glasses, J. Non-Cryst. Solids 522 (2019) 119580, https://doi.org/10.1016/j.jnoncrysol.2019.119580.

[39] M.I. Sayyed, A.A. Ali, M.H.A. Mhareb, K.A. Mahmoud, K.M. Kaky, Baki, M.A. Mahdi, Novel tellurite glass (60-x)TeO₂–10GeO₂ -20ZnO–10BaO - xBi₂O₃ for radiation shielding, J. Alloys Compd. 844 (2020) 155668, https://doi.org/10.1016/j.jallcom.2020.155668.

[40] K.M. Kaky, M.I. Sayyed, A.A. Ali, M.H.A. Mhareb, K.A. Mahmoud, S.O. Baki, Germanate oxide impacts on the optical and gamma radiation shielding properties of TeO₂-ZnO-Li₂O glass system, J. Non-Cryst. Solids 546 (2020) 120272, https://doi.org/10.1016/j.jnoncrysol.2020.120272.